Integral Equations for a Single Scatterer: Method of Moments and Rough Surfaces

1.1. Introduction

In this chapter, the integral equations (IEs) are addressed to derive the field scattered by a single scatterer in free space. They are obtained by introducing the Green function concept and by applying the boundary conditions onto the scatterer. In addition, the IEs are converted into a linear system by using the method of moments (MoM) with the point-matching method. The impedance matrix is then expressed for any shape of the object. The special case of a perfectly conducting (PC) object is also discussed. This chapter also presents the necessary statistical parameters to generate a random rough surface.

In all chapters, the media are considered as homogeneous, linear and isotropic. In addition, they are considered as non-magnetic, which means that the magnetic permeability is $\mu_0=4\pi\times 10^{-7}$ H/m. In addition, the medium Ω_0 (the subscript 0 is used for variables defined in vacuum) is considered as vacuum and the time convention $e^{-j\omega t}$ is used. Then, the derivative over the time t is $\partial/\partial t \rightarrow -j\omega$. For any media without sources, two Maxwell equations [KON 05, TSA 00] are simplified as:

$$\begin{cases} \mathbf{curl} \, \boldsymbol{H} = \boldsymbol{\nabla} \wedge \boldsymbol{H} = -j\omega \epsilon \boldsymbol{E} \\ \mathbf{curl} \, \boldsymbol{E} = \boldsymbol{\nabla} \wedge \boldsymbol{E} = j\omega \mu_0 \boldsymbol{H} \end{cases}$$
 [1.1]

where \boldsymbol{H} is the magnetic field and \boldsymbol{E} the electric field. In addition, ω is the pulsation (rad/s) and $\epsilon = \epsilon_0 \epsilon_r$ is the permittivity, in which $\epsilon_0 = 1/(36\pi \times 10^9)$

is the permittivity in vacuum and ϵ_r is the relative permittivity (which equals unity for vacuum). For a two-dimensional (2D) space of unitary vectors (\hat{x}, \hat{z}) , the vectorial operator ∇ is defined in Cartesian coordinates as:

$$\nabla = \frac{\partial}{\partial x}\hat{x} + \frac{\partial}{\partial z}\hat{z}.$$
 [1.2]

1.2. Integral equations

2

1.2.1. TE and TM polarizations and boundary conditions

Let \hat{n} be the normal to the surface S pointing toward Ω_0 and lying in the plane (\hat{x}, \hat{z}) (2D problem), and separating two media, Ω_0 (upper) and Ω_1 (lower), of dielectric permittivities ϵ_0 and ϵ_1 (see Figure 1.1), respectively.

For the transverse electric (TE) polarization (the electric field is normal to the incident plane (\hat{x}, \hat{z})), the electric field in the upper medium is defined as $E_0 = \psi_0 \hat{y}$, where ψ_0 is a scalar number. In medium Ω_0 , the use of equation [1.1] leads to:

$$\boldsymbol{H}_0 = \frac{1}{j\omega\mu_0} \boldsymbol{\nabla} \wedge \boldsymbol{E}_0 = -\frac{1}{j\omega\mu_0} \hat{\boldsymbol{y}} \wedge \boldsymbol{\nabla}\psi_0.$$
 [1.3]

knowing that $A_1 \wedge (A_2 \wedge A_3) = (A_1 \cdot A_3)A_2 - (A_1 \cdot A_2)A_3$, for any vectorial function A_i , we have:

$$\hat{\boldsymbol{n}} \wedge \boldsymbol{H}_{0} = -\frac{1}{j\omega\mu_{0}}\hat{\boldsymbol{n}} \wedge (\hat{\boldsymbol{y}} \wedge \nabla\psi_{0}) = -\frac{1}{j\omega\mu_{0}} \left[(\hat{\boldsymbol{n}} \cdot \nabla\psi_{0})\hat{\boldsymbol{y}} - (\hat{\boldsymbol{n}} \cdot \hat{\boldsymbol{y}})\nabla\psi_{0} \right]$$

$$= -\frac{\hat{\boldsymbol{y}}}{j\omega\mu_{0}} (\hat{\boldsymbol{n}} \cdot \nabla\psi_{0}), \qquad [1.4]$$

where $\hat{\boldsymbol{n}} \cdot \hat{\boldsymbol{y}} = 0$ since the normal lies in the plane $(\hat{\boldsymbol{x}}, \hat{\boldsymbol{z}})$. For the lower medium Ω_1 , the quantities \boldsymbol{E}_1 , \boldsymbol{H}_1 and ψ_1 also satisfy equation [1.4], in which the subscript "1" is used for variables defined in Ω_1 .

For a surface separating two dielectric media, the boundary conditions state that the electric and magnetic tangential fields are continuous. Since $E_{0,1} = \psi_{0,1}\hat{y}$, this leads from equation [1.4] to:

$$\begin{cases} \psi_0(\mathbf{r}) = \psi_1(\mathbf{r}) \\ \hat{\mathbf{n}} \cdot \nabla \psi_0(\mathbf{r}) = \hat{\mathbf{n}} \cdot \nabla \psi_1(\mathbf{r}) \end{cases}, \forall \mathbf{r} \in S.$$
 [1.5]

For the transverse magnetic (TM) polarization (the magnetic field is normal to the incidence plane (\hat{x}, \hat{z})), the magnetic field in the upper medium is defined as $H_0 = \psi_0 \hat{y}$. The use of equation [1.1] leads to:

$$\boldsymbol{E}_{0} = -\frac{1}{j\omega\epsilon_{0}} \boldsymbol{\nabla} \wedge \boldsymbol{H}_{0} = \frac{1}{j\omega\epsilon_{0}} \hat{\boldsymbol{y}} \wedge \boldsymbol{\nabla}\psi_{0},$$
 [1.6]

and

$$\hat{\boldsymbol{n}} \wedge \boldsymbol{E}_{0} = -\frac{1}{j\omega\epsilon_{0}} (\hat{\boldsymbol{y}} \wedge \boldsymbol{\nabla}\psi_{0}) \wedge \hat{\boldsymbol{n}} = +\frac{1}{j\omega\epsilon_{0}} \hat{\boldsymbol{n}} \wedge (\hat{\boldsymbol{y}} \wedge \boldsymbol{\nabla}\psi_{0})$$

$$= -\frac{1}{j\omega\epsilon_{0}} [(\hat{\boldsymbol{n}} \cdot \boldsymbol{\nabla}\psi_{0})\hat{\boldsymbol{y}} - (\hat{\boldsymbol{n}} \cdot \hat{\boldsymbol{y}})\boldsymbol{\nabla}\psi_{0}]$$

$$= +\frac{\hat{\boldsymbol{y}}}{j\omega\epsilon_{0}} (\hat{\boldsymbol{n}} \cdot \boldsymbol{\nabla}\psi_{0}).$$
[1.7]

Moreover, for the lower medium Ω_1 , $\boldsymbol{H}_1 = \psi_1 \hat{\boldsymbol{y}}$ and $\hat{\boldsymbol{n}} \wedge \boldsymbol{E}_1 = +\hat{\boldsymbol{y}}(\hat{\boldsymbol{n}} \cdot \nabla \psi_1)/(j\omega\epsilon_1)$. The boundary conditions state that the electric and magnetic tangential fields are continuous, leading to:

$$\begin{cases} \psi_0(\mathbf{r}) = \psi_1(\mathbf{r}) \\ \hat{\mathbf{n}} \cdot \nabla \psi_0(\mathbf{r}) = \frac{\epsilon_0}{\epsilon_1} \hat{\mathbf{n}} \cdot \nabla \psi_1(\mathbf{r}) \end{cases}, \forall \mathbf{r} \in S.$$
 [1.8]

In conclusion, for the TE and TM polarization, equations [1.5] and [1.8] lead to:

$$\begin{cases} \psi_0(\mathbf{r}) = \psi_1(\mathbf{r}) \\ \hat{\mathbf{n}} \cdot \nabla \psi_0(\mathbf{r}) = \rho_{01} \hat{\mathbf{n}} \cdot \nabla \psi_1(\mathbf{r}) \end{cases}, \forall \mathbf{r} \in S,$$
 [1.9]

where $\rho_{01}=1$ for the TE polarization and $\rho_{01}=\epsilon_0/\epsilon_1$ for the TM polarization.

1.2.2. Electric and magnetic currents for a 2D problem

For a 3D problem, the electric J_0 and magnetic M_0 currents are defined on the surface as:

$$\boldsymbol{J}_0 = \hat{\boldsymbol{n}} \wedge \hat{\boldsymbol{H}}_0, \ \boldsymbol{M}_0 = -\hat{\boldsymbol{n}} \wedge \hat{\boldsymbol{E}}_0, \tag{1.10}$$

where \hat{n} is the normal to the surface.

For the TE polarization, $E_0 = \psi_0 \hat{y}$ and from equation [1.4], we then have:

$$\begin{cases}
J_0 = -\frac{1}{j\omega\mu_0}\hat{\boldsymbol{n}}\wedge(\hat{\boldsymbol{y}}\wedge\nabla\psi_0) = -\frac{1}{j\omega\mu_0}(\hat{\boldsymbol{n}}\cdot\nabla\psi_0)\hat{\boldsymbol{y}} \\
\boldsymbol{M}_0 = -\hat{\boldsymbol{n}}\wedge(\psi_0\hat{\boldsymbol{y}}) = \psi_0(-\hat{\boldsymbol{n}}\wedge\hat{\boldsymbol{y}})
\end{cases}$$
[1.11]

For the TM polarization, $\boldsymbol{H}_0 = \psi_0 \hat{\boldsymbol{y}}$ and from equation [1.7], we then have:

$$\begin{cases}
\mathbf{J}_{0} = \hat{\mathbf{n}} \wedge (\psi_{0} \hat{\mathbf{y}}) = \psi_{0} (\hat{\mathbf{n}} \wedge \hat{\mathbf{y}}) \\
\mathbf{M}_{0} = -\frac{1}{j\omega\epsilon_{0}} \hat{\mathbf{n}} \wedge (\hat{\mathbf{y}} \wedge \nabla \psi_{0}) = -\frac{1}{j\omega\epsilon_{0}} (\hat{\mathbf{n}} \cdot \nabla \psi_{0}) \hat{\mathbf{y}}
\end{cases}$$
[1.12]

In conclusion, for the TE and TM polarizations, ψ_0 and the normal derivative $\hat{\boldsymbol{n}} \cdot \nabla \psi_0 = \partial \psi_0 / \partial n$ are related to the currents $\{\boldsymbol{M}_0, \boldsymbol{J}_0\}$ and $\{\boldsymbol{J}_0, \boldsymbol{M}_0\}$, respectively.

1.2.3. Huygens' principle and extinction theorem

In Figure 1.1, the upper medium Ω_0 stands for the domain bounded by the surface S and the contour $C_{0,\infty}$, whereas Ω_1 stands for the domain bounded by the surface S and the contour $C_{1,\infty}$. We recall that the normal to the surface \hat{n} pointed toward Ω_0 .

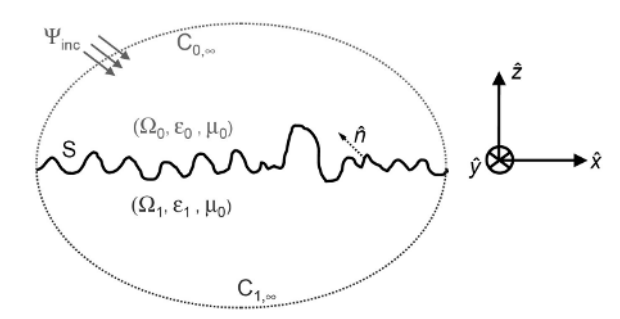


Figure 1.1. The domain Ω_0 is bounded by the contour $C_{0,\infty}$ and the surface S whereas Ω_1 is bounded by the contour $C_{1,\infty}$ and the surface S

In media Ω_0 and Ω_1 (without sources), the fields ψ_0 and ψ_1 satisfy the scalar Helmholtz equation:

$$\nabla^2 \psi_i(\mathbf{r}) + k_i^2 \psi_i(\mathbf{r}) = 0, \ \forall \mathbf{r} \in \Omega_i,$$
 [1.13]

where $k_i = \omega \sqrt{\epsilon_i \mu_0}$ is the wave number in medium Ω_i ($i = \{0, 1\}$) and ∇^2 is the scalar Laplacian. The scalar Green functions $g_0(\mathbf{r}, \mathbf{r}')$ and $g_1(\mathbf{r}, \mathbf{r}')$ defined in media Ω_0 and Ω_1 , respectively, satisfy:

$$\nabla^2 g_i(\mathbf{r}, \mathbf{r}') + k_i^2 g_i(\mathbf{r}, \mathbf{r}') = -\delta(\mathbf{r} - \mathbf{r}'), \tag{1.14}$$

where $\mathbf{r} = x\hat{\mathbf{x}} + z\hat{\mathbf{z}}$ are the Cartesian coordinates of the source point and $\mathbf{r}' = x'\hat{\mathbf{x}} + z'\hat{\mathbf{z}}$ are the Cartesian coordinates of the observation point. Physically, the Green function is the field radiated from a source point represented from the Dirac delta function δ . It then satisfies the Helmholtz equation, in which the right-hand side of equation [1.13] is $-\delta(\mathbf{r} - \mathbf{r}')$.

Applying the scalar Green theorem, we have:

$$\iint_{\Omega} (f_1 \nabla^2 f_2 - f_2 \nabla^2 f_1) dr = \oint_{C} (f_1 \nabla f_2 - f_2 \nabla f_1) \cdot d\mathbf{S}, \quad [1.15]$$

where $dS = \hat{n}dS$, in which \hat{n} is the unitary vector normal to the closed oriented contour bounding medium Ω .

Let $f_1 = \psi_0$ and $f_2 = g_0$ in equation [1.15]. Then, from equations [1.13] and [1.14], for $\mathbf{r} \in \Omega_0$ we have:

$$\iint_{\Omega_0} \left[\psi_0(\mathbf{r}) \nabla^2 g_0(\mathbf{r}, \mathbf{r}') - g_0(\mathbf{r}, \mathbf{r}') \nabla^2 \psi_0(\mathbf{r}) \right] d\mathbf{r}$$

$$= \iint_{\Omega_0} \left\{ \psi_0(\mathbf{r}) \left[-\delta(\mathbf{r} - \mathbf{r}') - k_0^2 g_0(\mathbf{r}, \mathbf{r}') \right] + g_0(\mathbf{r}, \mathbf{r}') k_0^2 \psi_0(\mathbf{r}) \right\} d\mathbf{r}$$

$$= -\iint_{\Omega_0} \psi_0(\mathbf{r}) \delta(\mathbf{r} - \mathbf{r}') d\mathbf{r}$$

$$= \begin{cases} -\psi_0(\mathbf{r}') \text{ if } \mathbf{r}' \in \Omega_0 \\ 0 \text{ if } \mathbf{r}' \notin \Omega_0 \end{cases}$$

$$= \int_{C_0} \left[\psi_0(\mathbf{r}) \nabla g_0(\mathbf{r}, \mathbf{r}') - g_0(\mathbf{r}, \mathbf{r}') \nabla \psi_0(\mathbf{r}) \right] \cdot d\mathbf{S}, \qquad [1.16]$$

where the contour $C_0 = S \cup C_{0,\infty}$ bounding the medium Ω_0 . In addition, the last line of equation [1.16] can be written as:

$$\int_{C_0} \left[\psi_0(\mathbf{r}) \nabla g_0(\mathbf{r}, \mathbf{r}') - g_0(\mathbf{r}, \mathbf{r}') \nabla \psi_0(\mathbf{r}) \right] \cdot d\mathbf{S}$$

$$= -\int_{S} \left[\psi_0(\mathbf{r}) \frac{\partial g_0(\mathbf{r}, \mathbf{r}')}{\partial n} - g_0(\mathbf{r}, \mathbf{r}') \frac{\partial \psi_0(\mathbf{r})}{\partial n} \right] dS$$

$$+ \int_{C_{0,\infty}} \left[\psi_0(\mathbf{r}) \frac{\partial g_0(\mathbf{r}, \mathbf{r}')}{\partial n} - g_0(\mathbf{r}, \mathbf{r}') \frac{\partial \psi_0(\mathbf{r})}{\partial n} \right] dS, \qquad [1.17]$$

where $\partial f/\partial n = \hat{\boldsymbol{n}} \cdot \boldsymbol{\nabla} f$. The minus sign before the integral over S is due to the sense of the normal $\hat{\boldsymbol{n}}$, which points inside Ω_0 . The plus sign before the integral over $C_{0,\infty}$ is due to the sense of the normal $\hat{\boldsymbol{n}}_{0,\infty}$, which points outside Ω_0 .

It can be shown that the integral over the contour $C_{0,\infty}$ equals minus the incident field $(-\psi_{\text{inc}}(\mathbf{r}'))$ [TSA 00]. For $\mathbf{r} \in S$, the substitution of equation [1.17] into equation [1.16] then leads to:

$$\begin{cases}
-\psi_{\text{inc}}(\mathbf{r}') = \int_{S} \left[\psi_{0}(\mathbf{r}) \frac{\partial g_{0}(\mathbf{r}, \mathbf{r}')}{\partial n} - g_{0}(\mathbf{r}, \mathbf{r}') \frac{\partial \psi_{0}(\mathbf{r})}{\partial n} \right] dS & \text{if } \mathbf{r}' \notin \Omega_{0} \\
\psi_{0}(\mathbf{r}') - \psi_{\text{inc}}(\mathbf{r}') = \int_{S} \left[\psi_{0}(\mathbf{r}) \frac{\partial g_{0}(\mathbf{r}, \mathbf{r}')}{\partial n} - g_{0}(\mathbf{r}, \mathbf{r}') \frac{\partial \psi_{0}(\mathbf{r})}{\partial n} \right] dS & \text{if } \mathbf{r}' \in \Omega_{0}
\end{cases}$$
(1.18)

Special attention must be paid when r' approaches the surface S from either below or above. For more details see [TSA 00 Chapter 4, section 2]. For $r' \notin \Omega_0$, equation [1.18] gives the *extinction theorem*. For $r' \in \Omega_0$ (S excluded), equation [1.18] gives the *Huygens' principle*:

$$\psi_{\text{sca},0}(\mathbf{r}') = \psi_0(\mathbf{r}') - \psi_{\text{inc}}(\mathbf{r}') = \int_S \left[\psi_0(\mathbf{r}) \frac{\partial g_0(\mathbf{r}, \mathbf{r}')}{\partial n} - g_0(\mathbf{r}, \mathbf{r}') \frac{\partial \psi_0(\mathbf{r})}{\partial n} \right] dS.$$
[1.19]

This shows that the scattered field $\psi_{\text{sca},0}$ is expressed from the field ψ_0 and its normal derivative on the surface $\partial \psi_0/\partial n$. These two quantities are often called *surface currents*.

Applying the same principle for the field ψ_1 in the lower medium Ω_1 , for $r \in S$ we have [TSA 00]:

$$\begin{cases}
0 = \int_{S} \left[\psi_{1}(\mathbf{r}) \frac{\partial g_{1}(\mathbf{r}, \mathbf{r}')}{\partial n} - g_{1}(\mathbf{r}, \mathbf{r}') \frac{\partial \psi_{1}(\mathbf{r})}{\partial n} \right] dS & \text{if } \mathbf{r}' \notin \Omega_{1} \\
\psi_{1}(\mathbf{r}') = -\int_{S} \left[\psi_{1}(\mathbf{r}) \frac{\partial g_{1}(\mathbf{r}, \mathbf{r}')}{\partial n} - g_{1}(\mathbf{r}, \mathbf{r}') \frac{\partial \psi_{1}(\mathbf{r})}{\partial n} \right] dS & \text{if } \mathbf{r}' \in \Omega_{1}
\end{cases}$$
[1.20]

and the scattered field $\psi_{\text{sca},1} = \psi_1$ since $\psi_{1,\text{inc}} = 0$ in Ω_1 . In equations [1.18] and [1.20], the four surface unknowns to determine on the surface are $\psi_0(\mathbf{r})$, $\partial \psi_0(\mathbf{r})/\partial n$, $\psi_1(\mathbf{r})$ and $\partial \psi_1(\mathbf{r})/\partial n$, whereas the quantities $\psi_{\text{inc}}(\mathbf{r}')$, $g_0(\mathbf{r}, \mathbf{r}')$ and $g_1(\mathbf{r}, \mathbf{r}')$ are known. It is therefore necessary to have two additional equations, which are obtained from the boundary conditions [1.9] on the surface S, valid $\forall (\mathbf{r}, \mathbf{r}') \in S$. Then, from equations [1.18] (the case for which is $\mathbf{r}' \in \Omega_0$), [1.20] (the case for which is $\mathbf{r}' \in \Omega_1$) and [1.9], $\forall (\mathbf{r}, \mathbf{r}') \in S$, the IEs are [TSA 00]:

$$\begin{cases}
\psi_{\text{inc}}(\mathbf{r}') = +\frac{1}{2}\psi_{0}(\mathbf{r}') - \int_{S} \psi_{0}(\mathbf{r}) \frac{\partial g_{0}(\mathbf{r}, \mathbf{r}')}{\partial n} dS + \int_{S} g_{0}(\mathbf{r}, \mathbf{r}') \frac{\partial \psi_{0}(\mathbf{r})}{\partial n} dS \\
0 = -\frac{1}{2}\psi_{0}(\mathbf{r}') - \int_{S} \psi_{0}(\mathbf{r}) \frac{\partial g_{1}(\mathbf{r}, \mathbf{r}')}{\partial n} dS + \int_{S} \frac{1}{\rho_{01}} g_{1}(\mathbf{r}, \mathbf{r}') \frac{\partial \psi_{0}(\mathbf{r})}{\partial n} dS
\end{cases} (1.21)$$

The symbol f stands for the Cauchy principal value, which means that the case ${\boldsymbol r}={\boldsymbol r}'$ is not accounted for in the calculation of the integral. In addition, letting $\int_S dS = \int dS + \int_P dS$ (where P is a piece), it is important to note that for ${\boldsymbol r}={\boldsymbol r}'\in S^+$ (at the upper limit), $\int_P \psi_0({\boldsymbol r}) \frac{\partial g_0({\boldsymbol r},{\boldsymbol r}')}{\partial n} dS = +\psi_0({\boldsymbol r}')/2$, and for ${\boldsymbol r}={\boldsymbol r}'\in S^-$ (at the lower limit), $\int_P \psi_0({\boldsymbol r}) \frac{\partial g_0({\boldsymbol r},{\boldsymbol r}')}{\partial n} dS = -\psi_0({\boldsymbol r}')/2$.

To solve a scattering problem, the currents on the surfaces ψ_0 and $\partial \psi_0/\partial n$ must be calculated. For an arbitrary shape of a surface, a numerically rigorous method is needed to compute them because the IEs have no analytical solution. This is discussed in the following section. From the knowledge of these currents, the scattered field $\psi_{i,\text{sca}}$ ($i=\{1,2\}$) is then computed in the domain $\Omega_i - S$ from equations [1.19] and [1.20] (with $r' \in \Omega_i$), respectively.

8

COMMENT 1.1.— 2D SCALAR GREEN FUNCTION—. For a 2D problem, the Green function is expressed as:

$$g_i(\mathbf{r}, \mathbf{r}') = \frac{j}{4} \mathbf{H}_0^{(1)}(k_i \|\mathbf{r} - \mathbf{r}'\|) = \frac{j}{4} \mathbf{H}_0^{(1)} \left[k_i \sqrt{(x - x')^2 + (z - z')^2} \right], [1.22]$$

where $H_0^{(1)}$ is the zeroth-order Hankel function of the first kind. Their derivatives with respect to x and z are then (with D = ||r - r'||):

$$\begin{cases}
\frac{\partial g_{i}(\mathbf{r}, \mathbf{r}')}{\partial x} = \frac{\partial g_{i}(k_{i}D)}{\partial D} \frac{\partial D}{\partial x} = -\frac{jk_{i}}{4} \mathbf{H}_{1}^{(1)}(k_{i}D) \frac{x - x'}{D} \\
\frac{\partial g_{i}(\mathbf{r}, \mathbf{r}')}{\partial z} = \frac{\partial g_{i}(k_{i}D)}{\partial D} \frac{\partial D}{\partial z} = -\frac{jk_{i}}{4} \mathbf{H}_{1}^{(1)}(k_{i}D) \frac{z - z'}{D}
\end{cases} (1.23)$$

The quantity $\partial g_i(\mathbf{r}, \mathbf{r}')/\partial n = \hat{\mathbf{n}} \cdot \nabla g_i(\mathbf{r}, \mathbf{r}')$ is then:

$$\frac{\partial g_i(\boldsymbol{r}, \boldsymbol{r}')}{\partial n} = -\frac{jk_i}{4} \frac{H_1^{(1)}(k_i \|\boldsymbol{r} - \boldsymbol{r}'\|)}{\|\boldsymbol{r} - \boldsymbol{r}'\|} (\boldsymbol{r} - \boldsymbol{r}') \cdot \hat{\boldsymbol{n}}.$$
 [1.24]

Figure 1.2 shows the real and the imaginary parts of $H_0^{(1)}(x)$ and its envelope versus x (x > 0). For $x \gg 1$, it behaves as a periodic function because for $x \to +\infty$, we have [ABR 70]:

$$H_0^{(1)}(x) \approx \sqrt{\frac{2}{x\pi}} \exp\left[j\left(x - \frac{\pi}{4}\right)\right] \text{ as } x \to +\infty.$$
 [1.25]

Moreover, the equation of its envelope is $\sqrt{2/(x\pi)} \propto \sqrt{1/x}$, which corresponds to a *cylindrical* wave (2D problem).

1.2.4. Radar cross-section (RCS)

For a 2D problem, in medium Ω_0 , the RCS is defined as:

$$RCS = \lim_{r' \to \infty} 2\pi r' \left| \frac{\psi_{\text{sca},0}}{\psi_{\text{inc},0}} \right|^2,$$
 [1.26]

where r' is the distance between the object (phase center) and the receiver.

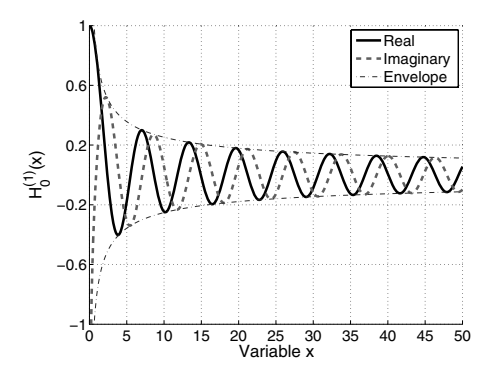


Figure 1.2. Real and the imaginary parts of $H_0^{(1)}(x)$ and its envelope versus x (x > 0)

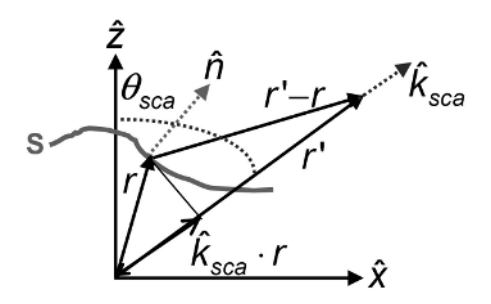


Figure 1.3. Huygens' principle in the far field for a 2D problem

As shown in Figure 1.3, in the far field $(r' \to \infty, r' \gg \text{and } r' \gg \lambda_0 = 2\pi/k_0)$, $\|r - r'\| = \|r' - r\| \approx r' - \hat{k}_{\text{sca}} \cdot r$ for the phase, whereas for the amplitude term $\|r - r'\| \approx r'$. From equation [1.25], in the observation direction defined by \hat{k}_{sca} , the Green function can be simplified in the far field as:

$$g_0(\mathbf{r}, \mathbf{r}') = \frac{j}{4} \mathbf{H}_0^{(1)}(k_0 \| \mathbf{r} - \mathbf{r}' \|) \approx \frac{j}{4} \sqrt{\frac{2}{\pi k_0 r'}} e^{j(k_0 r' - \mathbf{k}_{\text{sca}} \cdot \mathbf{r} - \pi/4)}.$$
 [1.27]

Moreover,

$$\frac{\partial g_0(\mathbf{r}, \mathbf{r}')}{\partial n} = \hat{\mathbf{n}} \cdot \nabla_{\mathbf{r}'} g_0(\mathbf{r}, \mathbf{r}') \approx -j g_0(\mathbf{r}, \mathbf{r}') \mathbf{k}_{\text{sca}} \cdot \hat{\mathbf{n}}.$$
 [1.28]

Substituting these two equations into the Huygens' principle [1.19], the scattered field in medium Ω_0 in the far-field zone (super script ∞) is:

$$\psi_{\text{sca},0}^{\infty} = \frac{j}{4} \sqrt{\frac{2}{\pi k_0 r'}} e^{-j\pi/4 + k_0 r'} \psi_{\text{sca},0}^{\infty,0} \psi_{\text{inc},0},$$
 [1.29]

where the variable $\psi_{\text{sca},0}^{\infty,0}$ is:

$$\psi_{\text{sca},0}^{\infty,0} = -\frac{1}{\psi_{\text{inc},0}} \int_{S} \underbrace{\left[j \boldsymbol{k}_{\text{sca}} \cdot \hat{\boldsymbol{n}} \psi_{0}(\boldsymbol{r}) + \frac{\partial \psi_{0}(\boldsymbol{r})}{\partial n} \right]}_{f(\boldsymbol{r})} e^{-j \boldsymbol{k}_{\text{sca}} \cdot \boldsymbol{r}} dS, \qquad [1.30]$$

and $\psi_{\text{inc},0}$ is the modulus of the incident field ψ_{inc} in medium Ω_0 . Then, the scattered far field is then obtained from the Fourier transform of f(r).

The substitution of equation [1.29] into equation [1.26] then leads to:

$$RCS = \frac{\left|\psi_{\text{sca},0}^{\infty,0}\right|^2}{4\left|k_0\right|}.$$
 [1.31]

Since $\psi_{\text{sca},0}^{\infty,0}$ is dimensionless, the RCS has the dimension of a distance (meter), since we consider it to be a 2D problem.

1.2.5. Normalized radar cross-section (NRCS)

If the surface has a finite extent, edge diffraction occurs, because the incident field does not vanish on the edges of the surface. To reduce this phenomenon, for the scattering from a rough surface, a tapered incident wave is used instead of a plane incident wave. A possible option is the Thorsos wave defined as [THO 88]:

$$\psi_{\text{inc}}(\boldsymbol{r}) = \psi_{\text{inc},0} \underbrace{\exp\left(j\boldsymbol{k}_{\text{inc}} \cdot \boldsymbol{r}\right)}_{\text{Plane wave}} \underbrace{\exp\left(-\frac{(x+z\tan\theta_{\text{inc}})^2}{g^2}\right)}_{\text{Damping factor}} \underbrace{\exp\left[jw(\boldsymbol{r})\boldsymbol{k}_{\text{inc}} \cdot \boldsymbol{r}\right]}_{\text{Corrective term}},$$

[1.32]

where

$$w(\mathbf{r}) = \left[\frac{2(x + z \tan \theta_{\text{inc}})^2}{g^2} - 1\right] \frac{1}{(k_0 g \cos \theta_{\text{inc}})^2},$$
 [1.33]

and $\mathbf{k}_{\text{inc}} = k_0(\sin\theta_i\hat{\mathbf{x}} - \cos\theta_i\hat{\mathbf{z}})$. The damping is orthogonal to the incident vector \mathbf{k}_{inc} . The additional corrective term allows us to better satisfy the Helmholtz equation. Nevertheless, the Thorsos wave verifies the Helmholtz equation at the order $\mathcal{O}\left(\frac{1}{(gk_0\cos\theta_{\text{inc}})^3}\right)$, implying that $1/C = gk_0\cos\theta_{\text{inc}} >> 1$. This condition is not satisfied for:

- grazing incidence angles: Indeed, for given k_0 and g, if $\theta_{\text{inc}} \to \pi/2$, then $gk_0 \cos \theta_{\text{inc}} \to 0$.
- -g small in comparison to the wavelength λ_0 : in other words, if the width of the incident beam is small in comparison to the wavelength.

Typically, $1/(gk_0\cos\theta_{\rm inc}) \leq C = 0.037$ and in the following, we take g = L/6, where L is the surface length.

From the Thorsos wave, the normalized incident power on the rough surface mean plane z=0 is then:

$$p_{\text{inc}} = -\frac{1}{|\psi_{\text{inc},0}|^2} \int_{-\infty}^{+\infty} S_{\text{inc}} \cdot \hat{z}|_{z=0} dx$$

$$= -\frac{1}{2|\psi_{\text{inc},0}|^2 \eta_0} \int_{-\infty}^{+\infty} |\psi_{\text{inc}}|^2 \hat{k}_{\text{inc}} \cdot \hat{z}|_{z=0} dx$$

$$= \frac{\cos \theta_{\text{inc}}}{2|\psi_{\text{inc},0}|^2 \eta_0} \int_{-\infty}^{+\infty} |\psi_{\text{inc}}|^2|_{z=0} dx$$

$$= \frac{g \cos \theta_{\text{inc}}}{2\eta_0} \sqrt{\frac{\pi}{2}} \left[1 - \frac{1 + 2 \tan^2 \theta_{\text{inc}}}{2k_0^2 g^2 \cos^2 \theta_{\text{inc}}} \right], \qquad [1.34]$$

where η_0 is the wave impedance in medium Ω_0 . In addition, S_{inc} is the Poynting vector that gives the power density carried by the incident wave. The NRCS is defined as [TSA 00]:

NRCS =
$$\lim_{r' \to \infty} \frac{r'}{2\eta_0} \frac{\left|\psi_{\text{sca},0}^{\infty}\right|^2}{p_{\text{inc}}} = \frac{1}{16\pi\eta_0 k_0} \frac{\left|\psi_{\text{sca},0}^{\infty,0}\right|^2}{p_{\text{inc}}},$$
 [1.35]

where the field $\psi_{\text{sca},0}^{\infty,0}$ is computed from equation [1.30]. Note that unlike the RCS, the NRCS is dimensionless.

1.3. Method of moments with point-matching method

The MoM is a numerical method that has been used extensively for the solution of scattering electromagnetic problems. Many excellent textbooks like [HAR 68, TSA 00] have been written on this subject. A characteristic of this technique is that it leads to a full matrix equation that can be solved from a matrix inversion. In this book, the MoM with point-matching method and pulse basis function is applied. Their main advantages are that they are simple to program and are efficient for scattering from rough surfaces.

Consider a 1D IE of the form:

$$\mathcal{L}\left(f\right) = g,\tag{1.36}$$

where \mathcal{L} is an integral operator or integral-differential operator, f is the unknown function and g is a given function.

- Step 1: Basis functions

A set of N basis functions in the domain \mathcal{D} is chosen. Let the basis functions be f_1, f_2, \ldots, f_N . The unknown function is expanded in terms of a linear combination of these functions:

$$f \simeq \tilde{f} = \sum_{n=1}^{N} a_n f_n, \tag{1.37}$$

and \tilde{f} verifies $\lim_{N\to+\infty}\left|f-\tilde{f}\right|=0$. The substitution of equation [1.37] into equation [1.36] leads to:

$$\mathcal{L}f = \mathcal{L}\left(\sum_{n=1}^{N} a_n f_n\right) + \varepsilon = g,$$
[1.38]

where ε is the residue due to the truncation of the sum at the order N. Since $\mathcal{L}f$ is a linear operator:

$$\mathcal{L}f = \sum_{n=1}^{N} a_n(\mathcal{L}f_n) + \varepsilon = g.$$
 [1.39]

- Step 2: Testing functions

Next, a set of M weighting functions w_1, w_2, \ldots, w_M is chosen. Multiplying equation [1.39] by $w_m(x)$ (with $m=1\ldots M$), assuming that $\langle w_m, \varepsilon \rangle \approx 0$ and integrating over the domain \mathcal{D} , we obtain:

$$\left\langle w_m, \sum_{n=1}^N a_n(\mathcal{L}f_n) \right\rangle = \sum_{n=1}^N a_n \left\langle w_m, \mathcal{L}f_n \right\rangle = \left\langle w_m, g \right\rangle,$$
 [1.40]

where the inner product $\langle \ldots \rangle$ is defined for a single variable x as:

$$\langle f, g \rangle = \int_{\mathcal{D}} f(x)g(x)dx.$$
 [1.41]

- Step 3: Linear system

From equation [1.40], the linear system to be solved is:

$$\bar{Z}X = b, ag{1.42}$$

in which the elements of the matrix \bar{Z} and the vector b are defined as:

$$\begin{cases}
Z_{mn} = \langle w_m, \mathcal{L}f_n \rangle \\
b_m = \langle w_m, g \rangle
\end{cases},$$
[1.43]

and the elements of the vector X, which equals a_n , must be determined. The matrix \bar{Z} is the impedance matrix of the scattering problem and depends on the shape and the electric properties of the surface.

- Point-matching method

Basis functions can use full domain functions such as sines, cosines, special functions, polynomials and modal solutions. A set that is useful for a practical problem is the subsectional basis function. This means that each f_n is only non-zero over a subsection of the domain of f.

A common choice is the pulse function:

$$f_n(x) = \begin{cases} 1 \text{ if } \alpha_n \le x \le \beta_n \\ 0 \text{ otherwise} \end{cases},$$
 [1.44]

where the interval \mathcal{D} is divided into N subintervals $\beta_n - \alpha_n$ with end points α_1 and β_N with $n = \{1, 2, ..., N\}$.

For the weighting functions w_m , the following are two common choices:

- 1) Galerkin's method. In this case, the weighting functions are the same as the basis function, that is $w_n(x) = f_n(x)$ with $n = \{1, 2, ..., N\}$.
- 2) Point-matching method. In this case, the weighting functions are the Dirac delta functions $w_m = \delta(x x_m)$ with $m = \{1, 2, ..., M\}$, and we choose M = N.

From the point-matching method and equation [1.40], we obtain:

$$Z_{mn} = \langle w_m(x), \mathcal{L}[f_n(x)] \rangle = \langle \delta(x - x_m), \mathcal{L}[f_n(x)] \rangle$$
$$= \int_{\mathcal{D}} \delta(x - x_m) \mathcal{L}[f_n(x)] dx = \mathcal{L}[f_n(x_m)],$$
[1.45]

and

$$b_m = \langle w_m, g(x) \rangle = \langle \delta(x - x_m), g(x) \rangle$$

= $\int_{\mathcal{D}} \delta(x - x_m) g(x) dx = g(x_m).$ [1.46]

1.4. Application to a surface

In this section, the MoM is applied along with the point-matching method to convert the IEs [1.21] into a linear system.

1.4.1. The Dirichlet boundary conditions

For a PC surface and for the TE polarization (the Dirichlet boundary conditions), the field vanishes on the surface, $\psi_0 = 0$. Thus, equation [1.21] can be simplified as:

$$\psi_{\text{inc}}(\mathbf{r}') = \int_{S} g_0(\mathbf{r}, \mathbf{r}') \frac{\partial \psi_0(\mathbf{r})}{\partial n} dS,$$
 [1.47]

where the points r = (x, y) and r' = (x', y') are on the surface S.

For a surface of length L and centered on x=0, equation [1.47] can be written as:

$$\mathcal{L}f = g, [1.48]$$

where

$$\begin{cases}
\mathcal{L} \bullet = \int_{-L/2}^{L/2} \sqrt{1 + \left(\frac{dz}{dx}\right)^2} g_0(\mathbf{r}, \mathbf{r}') dx \bullet \\
f = \frac{\partial \psi(\mathbf{r})}{\partial \mathbf{n}}, \quad g = \psi_{\text{inc}}(\mathbf{r}')
\end{cases}$$
[1.49]

The unknown is f. From the MoM, equation [1.47] is converted into a linear system $\bar{Z}X = b$. The elements of the impedance matrix \bar{Z} , Z_{mn} (with $(n,m) \in [1;N]$), and the components of the vector b, b_m , are given from equations [1.45] and [1.46] by:

$$Z_{mn} = \int_{\alpha_n}^{\beta_n} \sqrt{1 + \left(\frac{dz}{dx}\right)^2} g_0(\boldsymbol{r}, \boldsymbol{r}_m) dx$$

$$\approx \sqrt{1 + \left(\frac{dz_n}{dx_n}\right)^2} g_0(\boldsymbol{r}_n, \boldsymbol{r}_m) (\beta_n - \alpha_n), \qquad [1.50]$$

and

$$b_m = \psi_{\rm inc}(\boldsymbol{r}_m). \tag{1.51}$$

For the calculation of the integration over x of Z_{mn} , we assumed that the integrand does not vary significantly on the range $x \in [\alpha_n; \beta_n]$. Physically, this condition is fulfilled if $\beta_n - \alpha_n \ll \lambda_0$ (corresponding to slow variations of the Green function g_0 over the distance $\beta_n - \alpha_n$), where λ_0 is the wave length in medium Ω_0 . Typically, for the simulations $\beta_n - \alpha_n = \lambda_0/10$, corresponding to a distance for which the Green function slowly varies. For m = n, the Green function has a singularity. Then, the evaluation of integral [1.50] requires us to make Taylor series expansions of the integrand around $r = r_m$. For more

details, see [TSA 00, Chapter 4]. In conclusion, the elements of the impedance matrix are:

$$Z_{mn} = \frac{j\Delta_{n}\sqrt{1+\gamma_{n}^{2}}}{4} \begin{cases} \left[1 + \frac{2j}{\pi}\ln\left(0.164k_{0}\sqrt{1+\gamma_{n}^{2}}\Delta_{n}\right)\right] & \text{for } m = n\\ H_{0}^{(1)}(k_{0} \|\boldsymbol{r}_{n} - \boldsymbol{r}_{m}\|) & \text{for } m \neq n \end{cases}, [1.52]$$

where
$$||r_n - r_m|| = \sqrt{(x_n - x_m)^2 + (z_n - z_m)^2}$$

and

$$\begin{cases} X_n = \frac{\partial \psi(\mathbf{r}_n)}{\partial n}, \\ b_m = \psi_{\text{inc}}(\mathbf{r}_m) \end{cases},$$
[1.53]

with $\gamma_n = dz_n/dx_n$ and $\Delta_n = \beta_n - \alpha_n$.

1.4.2. The Neumann boundary conditions

For a PC surface and for the TM polarization (the Neumann boundary conditions), the normal derivative of the field vanishes on the surface, $\partial \psi_0/\partial n = 0$. Thus, equation [1.21] can be simplified as:

$$\psi_{\text{inc}}(\mathbf{r}') = \frac{1}{2}\psi_0(\mathbf{r}') - \int_S \psi_0(\mathbf{r}) \frac{\partial g_0(\mathbf{r}, \mathbf{r}')}{\partial n} dS,$$
 [1.54]

where the points r = (x, y) and r' = (x', y') are on the surface.

Using the same method as in the previous section and from equation [1.24], we have:

$$Z_{mn} = \begin{cases} -\frac{jk_0 \Delta_n}{4} \frac{\mathbf{H}_1^{(1)} (k_0 || \boldsymbol{r}_n - \boldsymbol{r}_m ||)}{\|\boldsymbol{r}_n - \boldsymbol{r}_m ||} \\ \times [\gamma_n (x_n - x_m) - (z_n - z_m)] \text{ for } m \neq n, & [1.55] \\ +\frac{1}{2} - \frac{\Delta_n}{4\pi} \frac{\gamma_n'}{1 + \gamma_n^2} & \text{for } m = n \end{cases}$$

where $\gamma_n' = \frac{d\gamma_n}{dx_n}$ and

$$\begin{cases}
X_n = \psi(\mathbf{r}_n) \\
b_m = \psi_{\text{inc}}(\mathbf{r}_m).
\end{cases}$$
[1.56]

1.4.3. General case

For a dielectric medium Ω_1 , equation [1.21] leads to:

$$\begin{cases} \psi_{\text{inc}}(\mathbf{r}') = \underbrace{+\frac{1}{2}\psi_0(\mathbf{r}') - \int_S \psi_0(\mathbf{r}) \frac{\partial g_0(\mathbf{r}, \mathbf{r}')}{\partial n} dS}_{\text{Neumann}} + \underbrace{\int_S g_0(\mathbf{r}, \mathbf{r}') \frac{\partial \psi_0(\mathbf{r})}{\partial n} dS}_{\text{Dirichlet}} \\ 0 = \underbrace{-\frac{1}{2}\psi_0(\mathbf{r}') - \int_S \psi_0(\mathbf{r}) \frac{\partial g_1(\mathbf{r}, \mathbf{r}')}{\partial n} dS}_{\text{Neumann with } k_0 \to k_1} + \underbrace{\int_S \frac{1}{\rho_{01}} g_1(\mathbf{r}, \mathbf{r}') \frac{\partial \psi_0(\mathbf{r})}{\partial n} dS}_{\text{Dirichlet with } k_0 \to k_1} . \quad [1.57] \end{cases}$$

The general case is then obtained from "linear combinations" of the Neumann and Dirichlet boundary conditions. The discretization of the above equations from the MoM then leads to the following impedance matrix:

$$\bar{Z} = \begin{bmatrix} \bar{Z}_{\text{Neu}} & \bar{Z}_{\text{Dir}} \\ \bar{Z}_{\text{Neu},k_0 \to k_1} & \frac{1}{\rho_{01}} \bar{Z}_{\text{Dir},k_0 \to k_1} \end{bmatrix},$$
 [1.58]

where the subscripts "Neu" and "Dir" mean Neumann and Dirichlet, respectively. It is important to note that for $\bar{Z}_{\mathrm{Neu},k_0\to k_1}$, the Cauchy principal value is -1/2, instead of +1/2 for \bar{Z}_{Neu} . In addition, the vectors b and X are:

$$\boldsymbol{b} = \begin{bmatrix} \psi_{\text{inc}}(\boldsymbol{r}_{1}) \\ \psi_{\text{inc}}(\boldsymbol{r}_{2}) \\ \vdots \\ \psi_{\text{inc}}(\boldsymbol{r}_{N}) \\ 0 \\ 0 \\ \vdots \\ 0 \end{bmatrix} N \text{ times} \end{bmatrix} \quad \text{and} \quad \mathbf{X} = \begin{bmatrix} \psi_{0}(\boldsymbol{r}_{1}) \\ \psi_{0}(\boldsymbol{r}_{2}) \\ \vdots \\ \psi_{0}(\boldsymbol{r}_{N}) \\ \frac{\partial \psi_{0}(\boldsymbol{r}_{1})}{\partial n} \\ \frac{\partial \psi_{0}(\boldsymbol{r}_{2})}{\partial n} \\ \vdots \\ \frac{\partial \psi_{0}(\boldsymbol{r}_{N})}{\partial n} \end{bmatrix}. \quad [1.59]$$

The square matrix \bar{Z} is of size $2N \times 2N$. The square matrices \bar{Z}_{Dir} and \bar{Z}_{Neu} of size $N \times N$ are expressed from equations [1.52] and [1.55], respectively.

For a dielectric media Ω_1 , the sampling step $\beta_n - \alpha_n$ is $(\lambda_0/10)/|\sqrt{\epsilon_{r1}}|$ instead of $\lambda_0/10$ for a PC surface because the wave number in medium Ω_1 is $k_1 = k_0\sqrt{\epsilon_{r1}}$, where k_0 is the wave number in a vacuum. Thus, for a highly conducting surface checking $\mathrm{Im}(\epsilon_{r1}) \gg 1$, the number of samples on the surface increases significantly, which makes the inversion of the impedance matrix very difficult. To overcome this issue, the impedance boundary condition (IBC) is applied.

1.4.4. Impedance boundary condition

For $\text{Im}(\epsilon_{r1}) \gg 1$, system [1.57] can be converted into only one IES. Indeed, from the Leontovitch boundary condition which is also called IBC, we have on the surface $r \in S$:

$$\begin{cases}
TE: \psi_0(\mathbf{r}) = \frac{j}{k_0} \sqrt{\frac{\epsilon_{r0}}{\epsilon_{r1}}} \frac{\partial \psi_0(\mathbf{r})}{\partial n} \\
TM: \frac{\partial \psi_0(\mathbf{r})}{\partial n} = \frac{k_0}{j} \sqrt{\frac{\epsilon_{r0}}{\epsilon_{r1}}} \psi_0(\mathbf{r})
\end{cases}$$
[1.60]

where $\text{Im}(\epsilon_{r1}) \gg 1$. System [1.57] is then simplified as:

$$\begin{cases}
TE: \psi_{inc}(\mathbf{r}') = \int_{S} \frac{\partial \psi_{0}(\mathbf{r})}{\partial n} \left[g_{0}(\mathbf{r}, \mathbf{r}') - \frac{j}{k_{0}} \sqrt{\frac{\epsilon_{r0}}{\epsilon_{r1}}} \frac{\partial g_{0}(\mathbf{r}, \mathbf{r}')}{\partial n} \right] dS \\
TM: \psi_{inc}(\mathbf{r}') = \frac{1}{2} \psi_{0}(\mathbf{r}') + \int_{S} \psi_{0}(\mathbf{r}) \left[g_{0}(\mathbf{r}, \mathbf{r}') \frac{k_{0}}{j} \sqrt{\frac{\epsilon_{r0}}{\epsilon_{r1}}} - \frac{\partial g_{0}(\mathbf{r}, \mathbf{r}')}{\partial n} \right] dS
\end{cases} .$$
[1.61]

For the TE polarization, it is important to note that the unknown is $\partial \psi_0({\bf r})/\partial n$ since $|\partial \psi_0({\bf r})/\partial n|\gg |\psi_0({\bf r})|$, which is similar to considering the Dirichlet boundary condition. On the other hand, for the TM polarization, the unknown is $\psi_0({\bf r})$ since $|\psi_0({\bf r})|\gg |\partial \psi_0({\bf r})/\partial n|$, which is similar to considering the Neumann boundary condition.

From the MoM, the matrix impedance is then:

$$\bar{Z} = \beta \bar{Z}_{Dir} + \alpha \bar{Z}_{Neu}, \qquad [1.62]$$

with

$$\begin{cases} \text{TE}: \beta = 1, & \alpha = \frac{j}{k_0} \sqrt{\frac{\epsilon_{r0}}{\epsilon_{r1}}}, \, \boldsymbol{X} = \frac{\partial \psi_0(\boldsymbol{r})}{\partial n}, \, \psi_0(\boldsymbol{r}) = \alpha \frac{\partial \psi_0(\boldsymbol{r})}{\partial n} \\ \text{TM}: \beta = \frac{k_0}{j} \sqrt{\frac{\epsilon_{r0}}{\epsilon_{r1}}}, \, \alpha = 1, & \boldsymbol{X} = \psi_0(\boldsymbol{r}), \quad \frac{\partial \psi_0(\boldsymbol{r})}{\partial n} = \beta \psi_0(\boldsymbol{r}) \end{cases} . \quad [1.63]$$

In conclusion, the use of the IBC allows us to discretize the surface along the wave number k_0 and then it becomes independent of the permittivity of medium Ω_1 . In terms of number of unknowns, it is equivalent to solving the scattering by a PC surface.

1.5. Forward-Backward (FB) method

For a problem with many unknowns, it is interesting to investigate rigorous fast numerical methods to treat the scattering from a large electrically rough surface. For instance, for a single rough surface, we can quote the banded-matrix-iterative-approach/canonical grid (BMIA-CAG) of Tsang et al. [TSA 93a, TSA 93b, TSA 95] of complexity $\mathcal{O}(N\log N)$, the FB method of Holliday et al. [KAP 96, ADA 96, HOL 98, IOD 02] of complexity $\mathcal{O}(N^2)$ and the accelerated version FB method with spectral acceleration (FB-SA) of Chou et al. [CHO 02, CHO 00, TOR 00, TOR 02] of complexity $\mathcal{O}(N)$, in which N is the number of unknowns on the surface.

In this section, the FB method is applied to a dielectric surface to speed up the calculation of $\bar{\mathbf{Z}}^{-1}\mathbf{b}$, in order to reduce the complexity to $\mathcal{O}(N^2)$ instead of $\mathcal{O}(N^3)$ from a direct lower–upper (LU) inversion.

We want to solve $\bar{Z}X = b \Leftrightarrow X = \bar{Z}^{-1}b$. From equation [1.58], the matrix \bar{Z} of size $2N \times 2N$ can be expressed from four square submatrices of size $N \times N$ as:

$$\bar{Z} = \begin{bmatrix} \bar{A} & \bar{B} \\ \bar{C} & \bar{D} \end{bmatrix}, \ X = \begin{bmatrix} X_1 \\ X_2 \end{bmatrix}, \ b = \begin{bmatrix} b_1 \\ b_2 \end{bmatrix}.$$
 [1.64]

The FB algorithm decomposes $\bar{Z}X = b$ into:

$$\begin{cases} \bar{A}_{\text{Diag}} \boldsymbol{X}_{1,\text{Forw}} + \bar{\boldsymbol{B}}_{\text{Diag}} \boldsymbol{X}_{2,\text{Forw}} = \boldsymbol{b}_1 - \bar{\boldsymbol{A}}_{\text{Forw}} \boldsymbol{X}_1 - \bar{\boldsymbol{B}}_{\text{Forw}} \boldsymbol{X}_2 \\ \bar{\boldsymbol{C}}_{\text{Diag}} \boldsymbol{X}_{1,\text{Forw}} + \bar{\boldsymbol{D}}_{\text{Diag}} \boldsymbol{X}_{2,\text{Forw}} = \boldsymbol{b}_2 - \bar{\boldsymbol{C}}_{\text{Forw}} \boldsymbol{X}_1 - \bar{\boldsymbol{D}}_{\text{Forw}} \boldsymbol{X}_2 \end{cases}, [1.65]$$

and

$$\begin{cases} \bar{A}_{\text{Diag}} X_{1,\text{Back}} + \bar{B}_{\text{Diag}} X_{2,\text{Back}} = -\bar{A}_{\text{Back}} X_1 - \bar{B}_{\text{Back}} X_2 \\ \bar{C}_{\text{Diag}} X_{1,\text{Back}} + \bar{D}_{\text{Diag}} X_{2,\text{Back}} = -\bar{C}_{\text{Back}} X_1 - \bar{D}_{\text{Back}} X_2 \end{cases}$$
[1.66]

For instance, \bar{A}_{Diag} is a diagonal matrix, \bar{A}_{Forw} a lower triangular matrix *upper* triangular matrix, all built $oldsymbol{A}_{\mathrm{Back}}$ $(\bar{A} = \bar{A}_{Forw} + \bar{A}_{Diag} + \bar{A}_{Back})$. The subscripts {Diag, Forw, Back} stand for diagonal, forward and backward matrices and are referred to as diagonal, and upper triangular matrices, respectively. $\{b_1, b_2, X_1, X_2\}$ are column vectors of length N. Finally, the unknown vectors are decomposed into $X_i = X_{i,Forw} + X_{i,Back}$ ($i = \{1, 2\}$), in which $X_{i,Forw}$ gives the forward contribution (from the points on the left of the current point) and $X_{i,\text{Back}}$ gives the *backward* contribution (from the *right*). The surface is oriented by assuming that the incident beam propagates from the left to the right.

To compute $X_i = X_{i,Forw} + X_{i,Back}$, an iterative procedure is applied. Assuming first that $X_{i,Back} = \mathbf{0} \Rightarrow X_i = X_{i,Forw} + X_{i,Back} = X_{i,Forw}$, equation [1.65] is solved for $X_{i,Forw}$. Then, by introducing $X_{i,Forw}$ in equation [1.66], we obtain $X_{i,Back}$. The first iteration $X_i^{(0)}$ is then equal to $X_{i,Forw} + X_{i,Back}$. The scheme is repeated to calculate the next iterations $X_i^{(p)}$ up to the order $p = P_{FB}$.

The use of equations [1.65] and [1.66] is very convenient to solve by substitution for $X_{i,\text{Forw}}$ and $X_{i,\text{Back}}$. For instance, from [1.65], since $\{\bar{A}_{\text{Forw}}, \bar{B}_{\text{Forw}}, \bar{C}_{\text{Forw}}, \bar{D}_{\text{Forw}}\}$ are lower triangular matrices with null diagonal coefficients, we get with $m \in [2; N]$:

$$\begin{cases} A_{\text{Diag}}^{m,m} X_{1,\text{Forw}}^m + B_{\text{Diag}}^{m,m} X_{2,\text{Forw}}^m = b_1^m - \sum_{n=1}^{n=m-1} \left(A_{\text{Forw}}^{m,n} X_1^n + B_{\text{Forw}}^{m,n} X_2^n \right) \\ \vdots \\ C_{\text{Diag}}^{m,m} X_{1,\text{Forw}}^m + D_{\text{Diag}}^{m,m} X_{2,\text{Forw}}^m = b_2^m - \sum_{n=1}^{n=m-1} \left(C_{\text{Forw}}^{m,n} X_1^n + D_{\text{Forw}}^{m,n} X_2^n \right) \end{cases}$$
[1.67]

For instance, $A^{m,n}$ is the element of the matrix \bar{A} of column m and row n. X_i^n is the nth component of the vector X_i . Thus, assuming first $X_{\text{Back}} = \mathbf{0} \Rightarrow X_i = X_{i,\text{Forw}} + X_{i,\text{Back}} = X_{i,\text{Forw}}$ and by solving equation [1.67], the unknowns $\{X_{1,\text{Forw}}^m, X_{2,\text{Forw}}^m\}$ with $m \in [2; N]$ are calculated from $4N^2/2$ multiplications. From equation [1.66], we obtain a similar equation system to [1.67] but the sum over n is $n \in [m+1; N]$, and the unknowns $\{X_{1,\text{Back}}^m, X_{1,\text{Back}}^m\}$ with $m \in [1; N-1]$ are also calculated from $4N^2/2$ multiplications. In conclusion, the complexity of the FB method is $\mathcal{O}(N^2)$.

Déchamps *et al.* [DÉC 07b] mathematically showed that the FB method converges if the spectral radius (i.e. the modulus of the eigenvalue, which has the highest modulus) of the characteristic matrix $\bar{M}_{c,\mathrm{FB}}$ is strictly smaller than 1, where $\bar{M}_{c,\mathrm{FB}}$ is expressed as:

$$\bar{\boldsymbol{M}}_{c,\mathrm{FB}} = (\bar{\boldsymbol{Z}}_{\mathrm{Diag}} + \bar{\boldsymbol{Z}}_{\mathrm{Forw}})^{-1} \, \bar{\boldsymbol{Z}}_{\mathrm{Forw}} \, (\bar{\boldsymbol{Z}}_{\mathrm{Diag}} + \bar{\boldsymbol{Z}}_{\mathrm{Back}})^{-1} \, \bar{\boldsymbol{Z}}_{\mathrm{Back}}.$$
 [1.68]

This method will be tested in Chapter 2.

1.6. Random rough surface generation

In this section, we describe how to generate realizations of a random rough surface. We assume that the surface is Gaussian, which means that the height probability density function (PDF) follows a Gaussian process or a normal law. We assume that the surface height profile z(x) is univocal and follows a stationary Gaussian random process.

1.6.1. Statistical parameters

For a centered Gaussian process, the surface height PDF is given by:

$$p_z(z) = \frac{1}{\sigma_z \sqrt{2\pi}} \exp\left(-\frac{z^2}{2\sigma_z^2}\right),$$
 [1.69]

and checks:

$$\begin{cases} \langle 1 \rangle = \int_{-\infty}^{\infty} p_z(z) dz = 1 \\ \langle z \rangle = \int_{-\infty}^{\infty} z p_z(z) dz = 0 \\ \langle (z - \langle z \rangle)^2 \rangle = \langle z^2 \rangle = \int_{-\infty}^{\infty} z^2 p_z(z) dz = \sigma_z^2 \end{cases}$$
 [1.70]

where

$$\langle \bullet \rangle = \int_{-\infty}^{\infty} (\bullet) p_z(z) dz.$$
 [1.71]

The real number σ_z stands for the surface height standard deviation and the surface height mean value $\langle z \rangle$ is zero. Since the height PDF is Gaussian, the derivative $d^n z(x)/dx^n$ also follows a Gaussian process.

Full characterization of the random rough surface height z is necessary for knowing the correlation between two heights on the surface of abscissa x_1 and x_2 . For z real, the surface height autocorrelation function is then defined as:

$$\langle z(x_1)z(x_1+x)\rangle = C_z(x).$$
 [1.72]

Since the process is stationary, C_z depends only on the abscissa difference $x=x_2-x_1$ between two points of the surface. Then, a Gaussian process is fully characterized by its height PDF, $p_z(z)$, and its surface height autocorrelation function, $C_z(x)$.

The power spectral density (PSD) or the surface height spectrum is defined as:

$$\hat{C}_z(k) = \text{FT}[C_z(x)] = \int_{-\infty}^{+\infty} C_z(x)e^{-jkx}dx,$$
[1.73]

and

$$C_z(x) = \frac{1}{2\pi} \text{FT}^{-1}[\hat{C}_z(k)] = \frac{1}{2\pi} \int_{-\infty}^{+\infty} \hat{C}_z(k) e^{jkx} dk,$$
 [1.74]

where FT denotes the Fourier transform.

From equations [1.74], [1.73], [1.72] and [1.70], we have:

$$\sigma_z^2 = C_z(0) = \frac{1}{2\pi} \int_{-\infty}^{+\infty} \hat{C}_z(k) dk.$$
 [1.75]

In addition, we can show that the surface slope autocorrelation function C_s is defined from the surface height autocorrelation function C_z as [BOU 99]:

$$C_s(x) = -\frac{d^2 C_z}{dx^2} = \frac{1}{2\pi} \int_{-\infty}^{+\infty} k^2 \hat{C}_z(k) e^{jkx} dx,$$
 [1.76]

and then the slope variance is:

$$\sigma_s^2 = C_s(0) = \frac{1}{2\pi} \int_{-\infty}^{+\infty} k^2 \hat{C}_z(k) dk.$$
 [1.77]

In addition, equation [1.77] shows that the surface slope spectrum is $\hat{C}_s(k) = k^2 \hat{C}_z(k)$.

1.6.2. Generation of a random profile

At the input of a linear filter, if e is a stationary process (of second order) of PSD \hat{C}_e , then the output signal s of PSD \hat{C}_s satisfies [KUN 91]:

$$\hat{C}_s = \left| \hat{C}_g \right|^2 \hat{C}_e, \tag{1.78}$$

where $\hat{C}_g = \mathrm{FT}(g)$ is the PSD of g, where g is the impulse response of the filter. In addition, if $\hat{C}_g \in \mathbb{R}^+$, then:

$$\hat{C}_g = \sqrt{\frac{\hat{C}_s}{\hat{C}_e}}. ag{1.79}$$

Since the system is assumed to be linear, we have [KUN 91]:

$$s = g * e = \mathrm{FT}^{-1}\left[\mathrm{FT}(g)\mathrm{FT}(e)\right] = \mathrm{FT}^{-1}\left[\sqrt{\frac{\hat{C}_s}{\hat{C}_e}}\,\mathrm{FT}(e)\right],\tag{1.80}$$

where the symbol * stands for the convolution product.

Since we want to generate a surface height Gaussian process z=s, a Gaussian white noise of unitary variance is applied at the input of the filter, which implies that $\hat{C}_e=1\ \forall k$. Then:

$$z = \mathrm{FT}^{-1} \left[\sqrt{\hat{C}_z} \, \mathrm{FT}(e) \right]. \tag{1.81}$$

Numerically, the convolution product is calculated in the Fourier domain because the complexity of a fast Fourier transform (FFT) is $\mathcal{O}(N \log N)$ instead of $\mathcal{O}(N^2)$ if the convolution product is calculated from its definition:

$$z(i) = g(i) * e(i) = \frac{1}{N} \sum_{n=1}^{N} g(n)e(n-i),$$
 [1.82]

where N is the length of both g and e. Since the surface height z is real, from equation [1.81], the function inside the operator FT^{-1} must satisfy $f^*(-k) = f(k) \ \forall k$, with * the complex conjugate operator. As shown further, \hat{C}_z is real and an even function of k. Thus, $\mathrm{FT}(e) = \hat{e}$ is a complex Gaussian white noise, which must satisfy $\hat{e}(-k)^* = \hat{e}(k)$. For more details, see [TSA 00, Chapter 4].

For surface height Gaussian and exponential autocorrelation functions defined as:

$$\begin{cases} C_z(x) = \sigma_z^2 \exp\left(-\frac{x^2}{L_c^2}\right) \\ C_z(x) = \sigma_z^2 \exp\left(-\frac{|x|}{L_c}\right), \end{cases}$$
 [1.83]

the surface height spectra (or PSD) are given from equation [1.73] by:

$$\begin{cases} \hat{C}_z(k) = \sigma_z^2 L_c \sqrt{\pi} \exp\left(-\frac{k^2 L_c^2}{4}\right) \\ \hat{C}_z(k) = \frac{2\sigma_z^2 L_c}{1 + k^2 L_c^2} \end{cases}.$$
 [1.84]

For an exponential autocorrelation function, its derivative is not defined for x=0. This implies, from equation [1.77], that the surface slope variance is not defined (from $-C_z''(0)$). On the other hand, it can be estimated from the spectrum of the generated surface $\hat{C}_z(k)$, because $\hat{C}_z(k)$ has a limited band, of upper cutoff spatial frequency k_c . Indeed, to have $k_c \to \infty$, the sampling step of the surface (generates from an FFT algorithm) must tend to zero since $\Delta x = \pi/(2k_c)$.

From equations [1.84], [1.83], [1.77] and [1.75], we can show for a Gaussian autocorrelation function that:

$$\begin{cases} \sigma_{z,k_c} \approx \sigma_{z,\infty} \text{erf}\left(\frac{k_c L_c}{2}\right) \\ \sigma_{s,k_c} \approx \sigma_{s,\infty} \left[\text{erf}\left(\frac{k_c L_c}{2}\right) - \frac{k_c L_c}{\sqrt{\pi}} \exp\left(-\frac{k_c^2 L_c^2}{4}\right) \right], \quad \sigma_{s,\infty} = \frac{\sigma_{z,\infty} \sqrt{2}}{L_c}, \quad [1.85] \end{cases}$$

and for an exponential autocorrelation function that:

$$\begin{cases}
\sigma_{z,k_c} = \sigma_{z,\infty} \sqrt{\frac{2 \arctan(k_c L_c)}{\pi}} \\
\sigma_{s,k_c} = \sigma_{s,\infty} \sqrt{1 - \frac{\arctan(k_c L_c)}{k_c L_c}}, \quad \sigma_{s,\infty} = \sigma_{z,\infty} \sqrt{\frac{2k_c}{\pi L_c}}.
\end{cases}$$
[1.86]

For $k_c \to \infty$, $\arctan(k_c L_c) \to \pi/2$ and $\arctan(k_c L_c)/(k_c L_c) \to 0$. Then, $\sigma_{z,\infty} = \sigma_z$ and $\sigma_{s,\infty} = \sigma_s$. Compared to a Gaussian autocorrelation function, the decreasing is slower since the function $\arctan(u)/u$ decreases more slowly than the functions $ue^{-u^2/4}/\sqrt{\pi}$ and $\operatorname{erf}(u/2)$.

For remote sensing applications, it is interesting to study the case of a sea surface. Under approximations [ELF 97], the sea surface can be modeled as a Gaussian process. For a 2D surface, the surface height autocorrelation function is defined from its spectrum as:

$$C_z(x,y) = \frac{1}{(2\pi)^2} \int_{-\infty}^{+\infty} \int_{-\infty}^{+\infty} \hat{C}_z(k_x, k_y) e^{jk_x x + jk_y y} dk_x dk_y.$$
 [1.87]

In addition, an ocean-like 2D spectrum is defined in polar coordinates (k_{ρ},ϕ) from $\hat{C}_z(k_x,k_y)dk_xdk_y=k_{\rho}\hat{C}_{z\rho}(\rho,\phi)dk_{\rho}d\phi=S(k_{\rho})[1+f(\phi)]dk_{\rho}d\phi$, where $S(k_{\rho})$ is the isotropic part of the sea spectrum and $f(\phi)$ is its anisotropic part. As $C_z(0,0)=\sigma_z^2$, we then have:

$$\sigma_z^2 = \frac{1}{(2\pi)^2} \int_{-\infty}^{+\infty} \int_{-\infty}^{+\infty} \hat{C}_z(k_x, k_y) dk_x dk_y$$

$$= \frac{1}{(2\pi)^2} \int_0^{2\pi} \left[1 + f(\phi) \right] \int_0^{\infty} S(k_\rho) dk_\rho$$

$$= \frac{1}{2\pi} \int_0^{\infty} S(k_\rho) dk_\rho,$$
[1.88]

since f is a periodic function over ϕ .

To set up a correspondence between a 2D spectrum $S(k_\rho)$ and 1D spectrum $\hat{C}_z(k)$, the comparison of equation [1.88] with equation [1.74] leads to $\hat{C}_z(|k|) = S(k_\rho)/2$ since \hat{C}_z is an even function of k. In the following, the spectrum of Elfouhaily *et al.* is used [ELF 97] for dealing with the case of a sea surface.

1.6.3. Simulations

In Figure 1.4, the surface height autocorrelation function is Gaussian of correlation length $L_c=10$ and of variance $\sigma_z=1$. a) The number of samples is N=8,192, and b) the number of samples is N=1,6384.

The top of Figure 1.4 shows that the surface heights (more precisely, $\operatorname{erf}(3/\sqrt(2)) = 99.7\%$ of heights) range from $-3\sigma_z$ to $+3\sigma_z$. As the correlation length decreases, the simulations show (not displayed here) that the surface is more irregular (the horizontal distance between two consecutive extrema decreases) because the surface slope variance increases. Theoretically, from equation [1.85], if L_c is divided by 2, then the slope variance $\sigma_{s,\infty}$ is multiplied by 2.

In the middle of Figure 1.4, the histograms show that z follows a Gaussian process and as the number of samples N increases, the histogram better matches the theoretical histogram (which is related to the height PDF by a normalization).

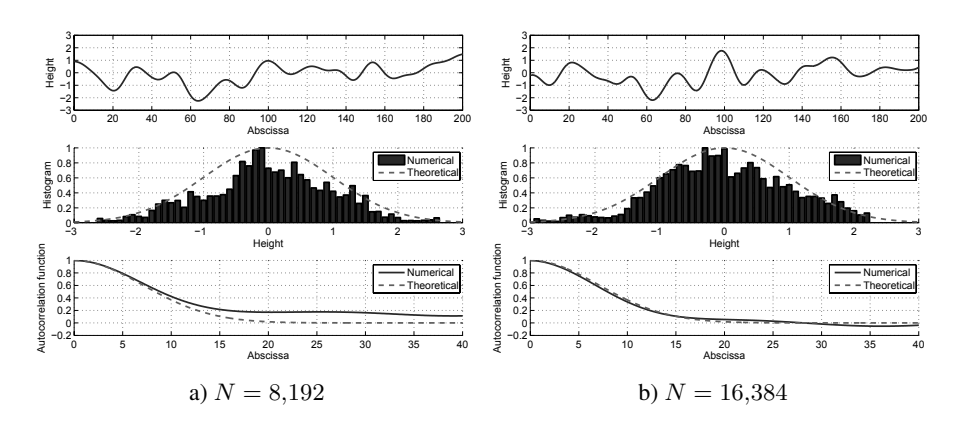


Figure 1.4. Top: Surface heights over $x \in [0; 200]$ versus the abscissa x. Middle: Height histogram versus the surface heights. Bottom: Surface height autocorrelation function versus the abscissa x. The surface height autocorrelation function is Gaussian of correlation length $L_c = 10$ and of variance $\sigma_z = 1$. a) The number of samples is N = 8,192, and b) the number of samples is N = 1,6384

The bottom of Figure 1.4 shows as N increases, the curve obtained numerically from z and equation [1.82] better matches the theoretical curve (equation [1.83]) for larger x. Indeed, as N increases, the length of the surface increases (with a constant sampling step) and then the correlation between far surface points is better predicted.

From Figure 1.5, the same remarks hold for an exponential autocorrelation function. The comparison of Figure 1.5 with Figure 1.4 shows that the surface is more irregular than that obtained from a Gaussian autocorrelation function, because the high frequencies contribute more to an exponential autocorrelation function. Indeed, as k increases, equation [1.84] shows that the corresponding spectrum decreases more slowly than that obtained from a Gaussian autocorrelation function. From an electromagnetic point of view, these high frequencies can have a strong impact on the scattered field.

Table 1.1 shows the values of the surface height and slope standard deviations, where σ_{z,k_c} and σ_{s,k_c} are computed from equations [1.85] and [1.86]. Moreover, $\tilde{\sigma}_z$ and $\tilde{\sigma}_s$ are computed from the generated surfaces shown in Figures 1.4 and 1.5. For the height variance, we can observe that σ_{z,k_c} is very close to $\tilde{\sigma}_z$ and the difference decreases as N increases. For the slope variance and for a Gaussian autocorrelation function, a good agreement is

also obtained between σ_{s,k_c} and $\tilde{\sigma}_s$, whereas the agreement is less good for an exponential autocorrelation function. In addition, as N increases, the slope variance does not change significantly with a Gaussian autocorrelation function, whereas with an exponential autocorrelation function, it changes significantly.

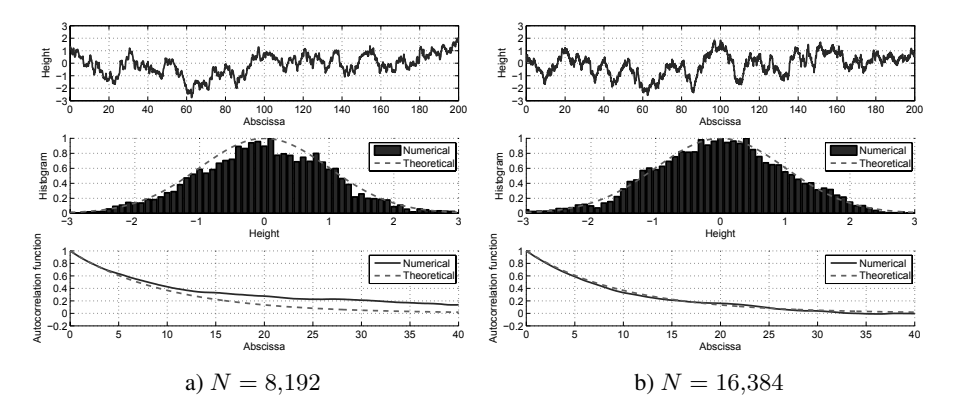


Figure 1.5. Same plots as in Figure 1.4 but for an exponential autocorrelation function

	N		σ_{z,k_c}		σ_{s,k_c}
	8,192				
	16,384				
Exponential					
Exponential	16,384	0.993	0.999	1.587	1.805

Table 1.1. Values of the surface height and standard deviations

The comparison of the surface heights and slopes computed from a sealike spectrum and a Gaussian autocorrelation function of the same height and slope variances is shown in Figure 1.6. The wind speed defined at 10 m above the sea is $u_{10}=5$ m/s, the number of samples is N=524,288 and the surface length is 400 m. Figure 1.6a) shows that the surface heights are similar, whereas the surface slopes strongly differ. Indeed, as shown in Figure 1.7, the sea slope spectrum contributes significantly to high wave numbers whereas for a Gaussian autocorrelation function, its slope spectrum rapidly decreases as k increases.

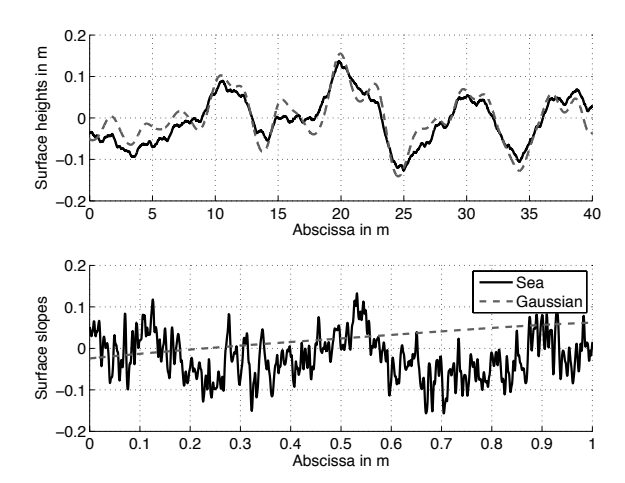


Figure 1.6. Top: Surface heights in m versus the abscissa x in m. Bottom: Surface slopes versus the abscissa x in m. For the sea spectrum, the wind speed $u_{10}=5$ m/s. The number of samples is N=524288 and the surface length is 400 m. For the Gaussian surface height autocorrelation function, the height variance σ_z^2 is the same as the sea surface and its associated correlation length L_c is computed from the sea surface slope variance σ_s^2 and equation [1.85] with $k_c \to \infty$

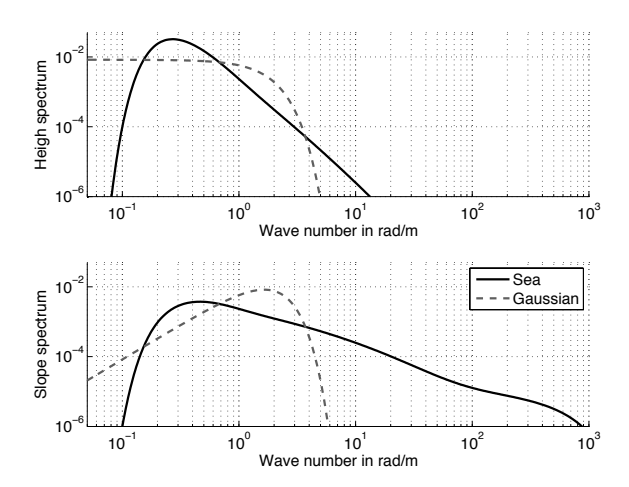


Figure 1.7. a) Surface height spectra \hat{C}_z versus the wave number k in rad/m. b) Surface slope spectra $\hat{C}_s = k^2 \hat{C}_z$ versus the wave number k in rad/m. Same parameters as in Figure 1.6

1.6.4. Conclusion

This section shows that the elevations of a random rough surface following a Gaussian process depend strongly on the choice of the height autocorrelation function. Indeed, two random rough surfaces having the same slope and height variances can strongly differ if the slope spectrum of one of the surfaces contributes to high frequencies. In fact, the surface variance (height, slope etc.) is obtained by integrating the corresponding spectrum over all the wave numbers, and cannot give the associated power for each frequency. When we want to properly characterize a natural surface (ocean, land, mountain, etc.), this point highlights that the knowledge of the surface height autocorrelation function or its spectrum is essential. Indeed, we will show in Chapter 2 that the high-frequency components of the surface can have a strong impact on the scattered field.